Revealing the hillslope response to earthquake legacy effect using time series InSAR

Nitheshnirmal Sadhasivam[1*], Ling Chang[2], Hakan Tanyaş[2]

[1] Department of Geosciences, Virginia Tech, Blacksburg, VA 24060, USA

[2] Faculty of Geo-Information Science and Earth Observation (ITC), University of Twente, Enschede, The Netherlands

*Corresponding authors: Nitheshnirmal Sadhasivam (nitheshnirmal@vt.edu)

ORCID ID, Nitheshnirmal Sadhasivam: 0000-0001-6502-8985

ORCID ID, Ling Chang: 0000-0001-8212-7221

ORCID ID: Hakan Tanyaş: 0000-0002-0609-2140

Abstract

Strong earthquakes are not only able to change the earth's surface processes by triggering a large population of coseismic landslides but also by influencing hillslope deformation rates in post-seismic periods. An increase in post-seismic hillslope deformation rates could also be linked to a change in post-seismic landslide hazard level and, thus, could be exploited to better assess post-seismic landslide risk in a given area. However, variations in hillslope deformations from pre- to post-seismic phases have rarely been examined for strong earthquakes. This paper examines pre- and post-seismic hillslope deformations, from 2014 to 2018, for a large area (~2,300 km^2) affected by the 2016 Mw7.8 Kaikōura earthquake using time series Interferometric Synthetic Aperture Radar (InSAR) techniques. To consistently analyze the entirety of the area from pre- to post-seismic phases, we aggregate InSAR-derived deformations for geomorphologically meaningful landscape partitions called Slope Units. We further examine the aggregated data through the hillslope deformation scheme, which we propose as a method to systematically identify the variations in post-seismic hillslope deformation trends. In this context, we label newly activated, uninterruptedly deforming, and stabilized hillslopes in the post-seismic phase. Our results show an ~130% increase in mean annual line-of-sight velocity after the earthquake. Overall, the areas affected by larger ground shaking show higher post-seismic deformations, which highlights the importance of the earthquake legacy effect as a factor controlling post-seismic hillslope deformations.

1. Introduction

Failure of hillslopes is one of the most common secondary geohazards associated with strong earthquakes (Fan et al., 2019). Nearly more than half of all seismic shaking-associated fatalities are caused by landslides (Marano et al., 2009; Nowicki Jessee et al., 2020). Furthermore, cascading effects of landslides keep affecting our lives in post-seismic periods, even years after earthquakes (Rosser et al., 2021). Therefore, identifying and monitoring the evolution of earthquake-triggered landslides in post-seismic periods is essential for disaster prevention, loss mitigation, and understanding how seismic activity impacts the regional landscape (Cai et al., 2022).

In spite of increasing research related to post-seismic landsliding (Chen et al., 2021; Kincey et al., 2021; Tang et al., 2016), our knowledge of sub-meter deformation of active hillslopes during the post-seismic phase is considerably lesser. Specifically, strong ground shaking during earthquakes could create widespread fissures/tension cracks on the slope materials. These newly generated discontinuity surfaces could decrease the hillslope strength and cause slow movement that displays no indication of rapid slope failure (Petley et al., 2010). Moreover, strong seismic shaking not only triggers coseismic landslides but also exacerbates hillslope stability in the post-seismic periods (Brain et al., 2017; Parker et al., 2015). This causes an increase in the post-seismic landslide susceptibility or hazard level, which relates to the earthquake legacy effect (Fan et al., 2019; Tang et al., 2016; Tanyaş et al., 2021b). However, there is limited literature on such incipient slow-moving landslides triggered by powerful earthquake shaking so far. For instance, Rosser et al. (2021) observed such cracks after the 2015 Gorkha earthquake and hinted at the possible development of slow-moving landslides triggered by the earthquake.

So far, our understanding of earthquake legacy effect on post-seismic landsliding and their recovery time is mainly based on the examination of landslide inventories, while the same has not been yet elaboratively analyzed by identifying, mapping, and monitoring dynamics of active or slow-moving hillslopes. In fact, variations in surface deformations during pre- and post-seismic phases provide a more comprehensive picture of the earthquake legacy effect and its evolution over time than multi-temporal landslide inventories because surface deformation could exist regardless of landslide occurrences. Moreover, understanding how slow-moving hillslopes originate/evolve after a common triggering event such as an earthquake can help us assess the post-seismic landslide hazard in a more robust way to plan preventive measures and reduce the risk from rapid catastrophic failure (Palmer, 2017; Intrieri et al., 2018).

Spaceborne SAR (Synthetic Aperture Radar) provides a unique tool to capture hillslope deformations (Bamler and Hartl, 1998). SAR-based landslide observation and modelling began way back in the middle of the 1990s (Fruneau et al., 1996), but only at the beginning of the 21st century did InSAR (Interferometric SAR) become famous for monitoring landslide deformations (Ferretti et al., 2001; Berardino et al., 2002; Hooper et al., 2004; Hooper, 2008; Meisina et al., 2006). Particularly time series InSAR (TS-InSAR), such as PSI (Persistent Scatterer Interferometry) and SBAS (Small BAseline Subset) approaches, are the most frequently applied techniques for landslide deformation analysis in recent years (Bayer et al., 2017; Tantianuparp et al., 2013; Zhao et al., 2018). The TS-InSAR applications largely transformed the process of landslide monitoring and hugely aided researchers in understanding the evolution of slowly deforming hillslopes (Bayer et al., 2017; Colesanti et al., 2003; Colesanti and Wasowski, 2006; Handwerger et al., 2015; Hilley et al., 2004; Wasowski and Bovenga, 2014; Bekaert et al. 2020). It can be used to unveil the smallest of displacements that are happening within a slope. However, owing to the high computational requirement of TS-InSAR techniques, regional scale analyses, in particular, associated with earthquakes, are still rare. For instance, Lacroix et al. (2022) revealed the lagged initiations and post-seismic relaxations of slow-moving landslides in the area hit by the 2015 Gorkha earthquake using Sentinel-1 SAR data. During this post-seismic relaxation phase, slow-moving hillslopes were found to have accelerating deformation mainly because of groundwater transmission. Also, Martino et al. (2022) showed slow activations and reactivations of landslides following an earthquake of magnitude (Mw = 5.1) in Italy with the help of the Differential InSAR technique. Cheaib et al. (2022) uncovered three distinct post-seismic deformation pattern hillslopes affected by ground motion from the 2017 Sarpol Zahab earthquake (Mw = 7.3): (i) post-seismic motion identical to pre-seismic level, (ii) steady increase in the post-seismic deformation velocity, and (iii) temporary increase in post-seismic velocity, which recovers to pre-seismic level in some time after the earthquake. Cai et al. (2022) exploited SBAS and laser scanning techniques to identified 16 slowly moving landslides that were developed after the Mw = 7 2017 Jiuzhaigou earthquake. Moreover, Cao et al. (2022) identified multiple slow-moving landslides that were generated from the intense ground shaking during the 2016 Kaikōura earthquake.

The literature implies that there is a growing interest in the geoscientific community for unveiling the dynamics of incipient slow-moving hillslopes that are triggered by strong earthquakes. This study will contribute to this notion. Specifically, in this research, a new systematic PSI-based approach is designed by integrating various pre- and post-processing steps to detect and study the sub-meter deformation evolution of active hillslopes that existed before and those that are generated after the 2016 Mw= 7.8 Kaikōura earthquake using the freely available Sentinel-1 SAR dataset. To systematically examine the large subset of the area affected by the earthquake, we propose to follow a novel approach of aggregating InSAR-derived deformations for every hillslope partition called Slope Unit (SU), as an alternative to commonly used pixel clustering methods (Aslan et al., 2020; Bekaert et al., 2020). Ultimately, to consistently analyze post-seismic hillslope evolution, we develop a hillslope deformation scheme (HDS), which could also be applied in any other earthquake-affected areas to classify sub-meter hillslope deformation activity before and after an earthquake. Unlike the landslide activity matrix suggested by Cigna et al. (2013), which requires pre-existing inventory, HDS does not require a pre-existing inventory and is less intricate to understand and for applying in earthquake-impacted hillslopes.

2. Study area and data description

In this study, we chose to focus on hillslopes in a region affected by the 7.8 Mw Kaikōura earthquake, which hit the north-eastern region of New Zealand's Southern Island on 14 November 2016 at local time 12:03 am (Figs. 1a and 1b). Earthquake hypocentre was located at 15.1 km depth and the rupture originated from 42.69°S, 173.02°E (Duputel and Rivera, 2017). The earthquake displayed the most complex rupturing mechanism ever recorded, involving more than 11 fault planes (Hamling et al., 2017). There has been no such large magnitude earthquake documented in the history of New Zealand for over 100 years (Ulrich et al., 2019). Displacements over 8 m have been observed in some regions of the Southern Island (Hamling et al., 2017). The losses attributed to the event were around 1.8 to 4.9 billion (Bradley et al., 2017).

Among the wide area affected by the 2016 Kaikōura earthquake, the particular region investigated in this work, with ~2,300 km^2 spatial extent (outlined by the yellow rectangle in Fig. 1c), is chosen mainly (i) to exploit freely available Sentinel-1 SAR images and (ii) to examine the main area affected the 2016 Kaikōura earthquake, which also hosts more than 50% of coseismic landslides. Specifically, Tanyas et al. (2022a) mapped ~4,000 coseismic landslides, and our study area covers 7,159 of them.

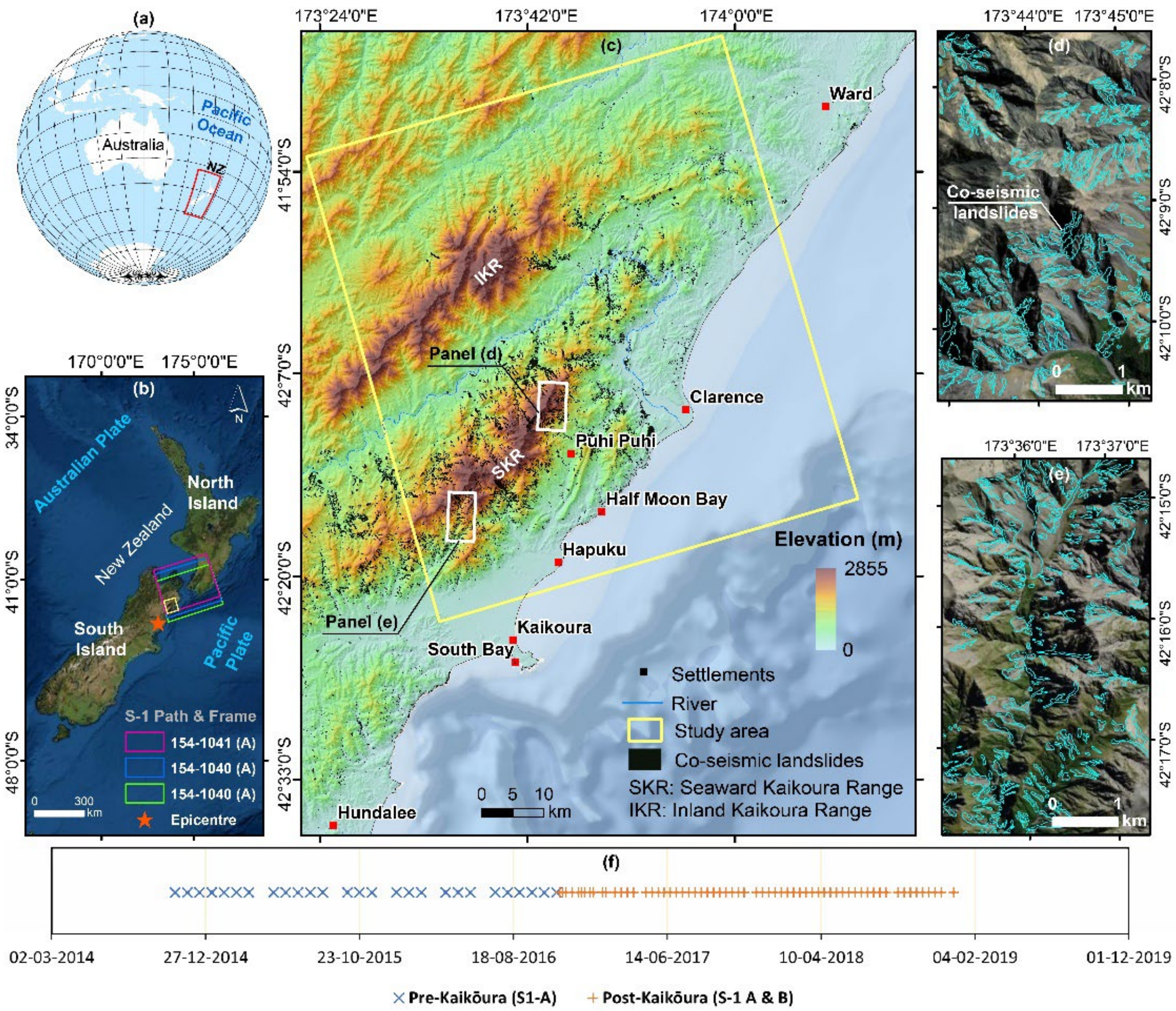

Fig. 1. Study area. (a) Insert map showing the geographical situation of New Zealand in the world map, (b) the location of study area in New Zealand along with the Sentinel-1 SAR scenes covering the study area, and (c) physiographical setting and coseismic landslide distribution of the study area affected by the 2016 M_w = 7.8 Kaikōura earthquake. Panels (d) and (e) show zoomed-in view of coseismic landslide polygons (Tanyaş et al., 2022a). Panel (f) shows the distribution of examined Sentinel-1 SAR images over time for pre-Kaikōura (x-marks in blue) and post-Kaikōura periods (Plus signs in orange) in ascending direction. SKR: the Seaward Kaikōura Ranges; IKR: the Inland Kaikōura Range.

We examined 90 Sentinel-1 SAR data available between October 2014 and December 2018 in descending direction (Fig. 1b and Table 1). To obtain coherent radar scatterers as much as possible and avoid temporal decorrelation, the analysis period was split into two intervals (e.g., Braun et al., 2020) as pre- and post-seismic periods (Fig. 1f and Table 1).

Sentinel-1 A and B, which have been active from 2014 and 2016 onwards, nominally have 6 to 48 day repeat cycle. For our case, the interval between two adjacent images majorly varies between 24 and 48 days in the case of the pre-seismic period, while the interval becomes shorter with most images acquired between an interval of 6 or 12 days in the post-seismic period.

Table 1. Key information of Sentinel-1 (S-1) SAR data utilized in this study (Pol.: Polarimetric channel).

Period	Sensor	Direction	Pol.	Path	Frame / Image count	Start date/ End date	# images
Pre-Kaikōura	S-1A	Ascending	VV	154	1040 / 14 1041 / 13	28-10-2014 to 10-11-2016	27
Post-Kaikōura	S-1A S-1B	Ascending	VV	154	1041 / 4 1040 / 3 & 1041 / 56	16-11-2016 to 24-12-2018	63

This study used Generic Atmospheric Correction Online Service (GACOS, Yu et al., 2018) provided by Newcastle University for eliminating the atmospheric phase delays in SAR interferograms. We used the void filled Shuttle Radar Topography Mission (SRTM) DEM of 1-arc second to assess the role of various DEM derivatives in hillslope deformation. Also, to evaluate the contribution of ground shaking associated with the 2016 Kaikōura earthquake, we used the U.S. Geological Survey (USGS) ShakeMap's Peak Ground Acceleration (PGA) estimate (Worden and Wald, 2016).

3. Methodology

Overall, the methodology of this study consists of seven steps: (i) pre-processing of PSI (single-master interferogram formation), (ii) PSI processing, (iii) analysis of the spatial distribution of PS across different landscape characteristics, (iv) detection of actively deforming PS points, (v) identification of active hillslopes during pre- and post- seismic phases, (vi) examining the sub-meter hillslope deformation evolution based on proposed HDS and (vii) probing the recovery of earthquake initiated active hillslope deformation. The complete workflow of this study is presented in Fig. 2.

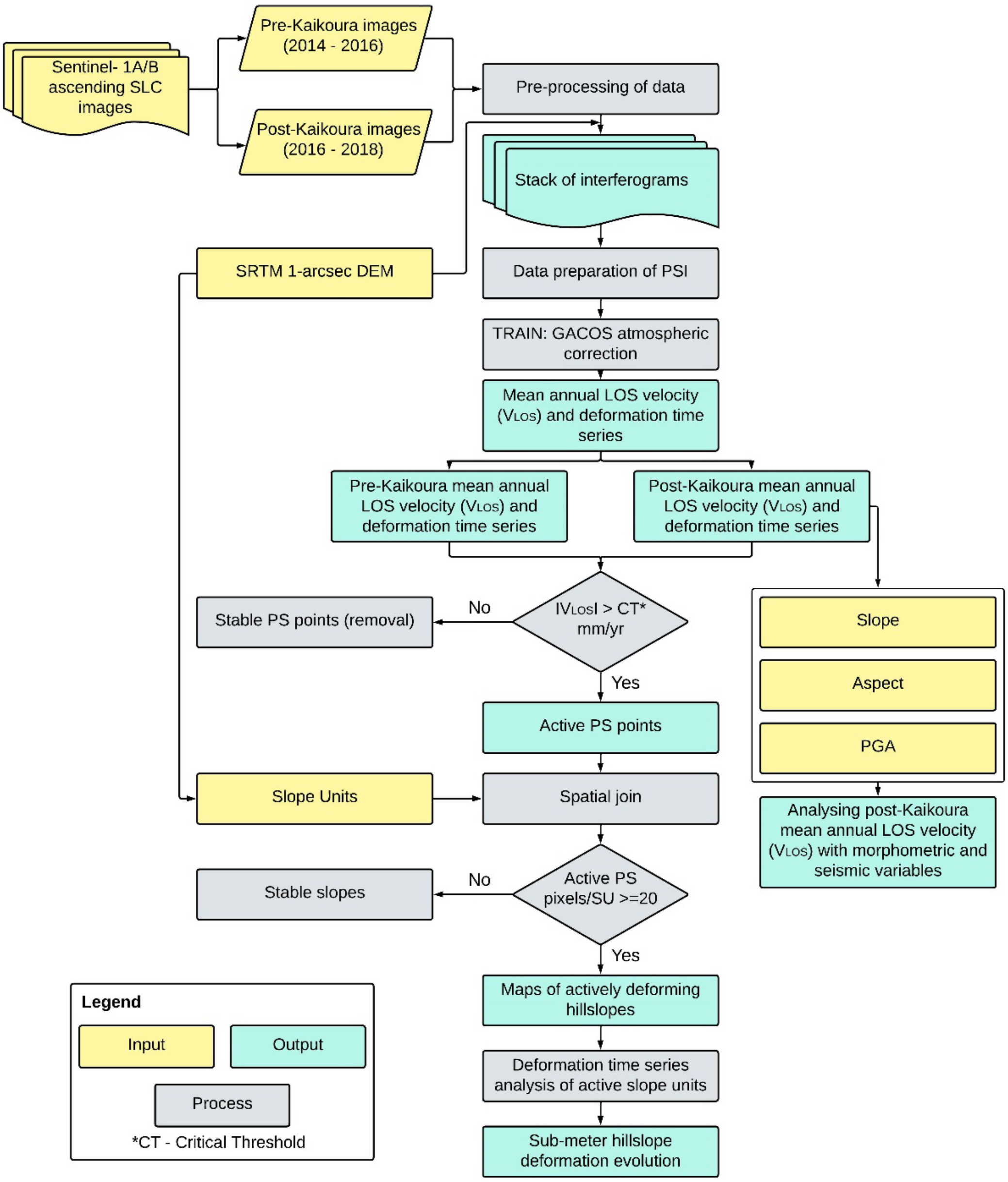

Fig. 2. General synopsis of the methods.

3.1. Pre-processing and Persistent Scatterer Interferometery (PSI) processing

Both pre-processing and PSI processing are run separately for the pre- and post- Kaikōura phases. For the automated generation of Sentinel-1 interferograms, the open-source SNAP2StaMPS python tool developed by Blasco et al. (2018) is used, which repeatedly calls the graphs created from the graph processing tool (GPT) of SentiNel Application Platform (SNAP version 8.0.0). This python-based SNAP2StaMPS tool is implemented in the Jupyter Notebook IDE on a 32 vCPU Intel ×86-64, 768 GB RAM, NVIDIA RTX A4000 GPU computing unit. The stacks of interferograms are the output prepared for further Stanford Method for Persistent Scatterers (StaMPS, Hooper et al., 2012; Hooper, 2008) based PSI processing. To properly remove the atmospheric phase, GACOS is employed with the help of TRAIN (Toolbox for Reducing Atmospheric InSAR Noise, Bekaert et al., 2015). The final products are deformation time series of all PS and mean annual line-of-sight (LOS) velocity (V_{LOS}) maps. The details for extracting surface deformation from the Sentinel-1 SLC dataset with VV polarization, including pre-processing and processing stages of PSI, are provided in the Supplementary Materials.

3.2. Spatial distribution of PS over morphometric and seismic variables

We examine the spatial distribution of PS derived for the post-seismic period in relation to the morphometric and seismic variable for understanding their association. More specifically, the hillslope steepness and aspect are examined in relation to all PS and their velocity. These variables provide insights about the hillslope geometry and serve as an indicator in addressing the balance of stability factors acting on a hillslope and study area as a whole (McColl, 2022). As for the seismic influence, PGA estimates of the 2016 Kaikōura earthquake is examined with the PS showing the mean annual V_{LOS}.

3.3. Detection of actively deforming PS points and hillslopes

Following the generation of surface deformation time series, PS points are methodically evaluated for identifying actively deforming points (Raspini et al., 2018). We mainly focus on PS deformation trend change over time and determine a critical stability threshold to the deformation velocity that can aid in identifying those potential actively deforming points. By following such a procedure, stable points can be eliminated for further analysis (e.g., Aslan et al., 2020).

For identifying actively deforming points, there are two commonly used methods in literature: (i) setting a critical stability threshold of either one or two standard deviations for PS velocity (Aslan et al., 2020; Bekaert et al., 2020) and (ii) using the hillslope velocity classification of Cruden and Varnes (1996). In the case of the former method, those PS points whose absolute velocities are more than 1 or 2 standard deviations (σ) are mostly considered 'active', and the rest are considered 'stable'. In the latter method, for instance, Cigna et al. (2013) characterized those hillslopes having active deformation to be extremely slow-moving ($|\pm 13|$ mm/yr ≤ V_{LOS} < $|\pm 16|$ mm/yr) and very slow-moving hillslopes (V_{LOS} ≥ $|\pm 16|$ mm/yr) based on Cruden and Varnes (1996) classification. Even though there is no lower threshold coined for extremely slow-moving hillslopes in Cruden and Varnes (1996) classification, the authors made an assumption in setting $|\pm 13|$ mm/yr as the minimum threshold.

This research proposes to couple both approaches summarized above to differentiate active PS from stable ones. In particular, we set the common critical stability threshold as $|\pm 10|$

mm/yr. This assumption well aligns with the literature (e.g., 13 mm/yr in Cigna et al., 2013) and the dataset we examined in which the one standard deviation of mean LOS (line-of-sight) velocities from post-Kaikōura phase is 8.44 mm/yr. Therefore in this study, those PS having mean LOS velocities equal to or greater than |±10| mm/yr are classified as active points, while the rest are excluded as they are stable. Moreover, this procedure can aid us in removing pixels that are affected by shadow effects (Bekaert et al., 2020). In addition, active PS is also sub-categorized as extremely slow-moving (|±10| mm/yr ≤ V_{LOS} < |±16| mm/yr) and very slow-moving (V_{LOS} ≥ |±16| mm/yr) PS (Cruden and Varnes, 1996). We should also stress that PS pixels that are located below 10 degrees of slope are eliminated as they are not mostly associated with the hillslope deformation.

To systematically examine InSAR-derived hillslope deformations over the entire study area, we use r.slopeunits software and delineate Slope Units (SUs), which are mapping units representing those regions that have similar slope and aspect (Alvioli et al., 2018). In other words, partitions of terrain displaying homogeneity in terms of slope and aspect are delineated as a SU. These units represent what geomorphologists widely accept as a natural hillslope, and it is widely used in landslide susceptibility/hazard modelling (Guzzetti et al., 2005). Earlier studies had aggregated a cluster of significant coherent scatterers lying on a study site that displays active deformation to be slow-moving hillslopes rather than considering any terrain unit since processes that occur within a slope is mostly discrete (Bekaert et al., 2020). Although SUs have been in use for landslide studies since 1988, it has been rarely used for identifying slowly moving hillslopes in combination with InSAR techniques (López-Vinielles et al., 2021).

After generating SUs, we count the number of active PS points within each of them. At this point, a PS threshold is defined to identify if a SU is slowly moving or not. Such an approach increases the reliability that the active deformations of PS are associated with hillslope processes and are not because of any individual unstable structures (Notti et al., 2014). Cigna et al. (2013), López-Vinielles et al. (2021), and Pawluszek-Filipiak et al. (2021) suggested that at least three to five actively deforming PS should be utilized for identifying a slow-moving hillslope. However, in this study, we safely assume that those slope units which contain ≥ 20 active PS are classified as slow-moving. We then calculate average deformations and annual LOS deformation velocities for SUs to further classified them as extremely slow-moving and very slow-moving hillslopes. In addition, we investigate deformation time series to capture continuous displacement patterns proving the existence of actively deforming hillslopes.

3.4. Post-seismic hillslope deformation scheme

In order to define the different states of sub-meter hillslope deformation activity before and after the Kaikōura earthquake, we propose a post-seismic hillslope deformation scheme (HDS) (Fig. 3). The average V_{LOS} of the entire hillslopes is used to define the state of activity of a hillslope. It is assumed that four different types of hillslope activities can be captured by the proposed activity matrix. Type I describes those hillslopes that are stable in the pre-seismic phase, which become active in the post-seismic period (Lacroix et al., 2014). Type II refers to actively deforming hillslopes that continue being actively deforming in the post-seismic period (Bekaert et al., 2020). Type III indicates actively deforming hillslopes that become stable during the post-seismic period. Finally, Type IV refers to hillslopes that remain stable during pre- and post-seismic phases.

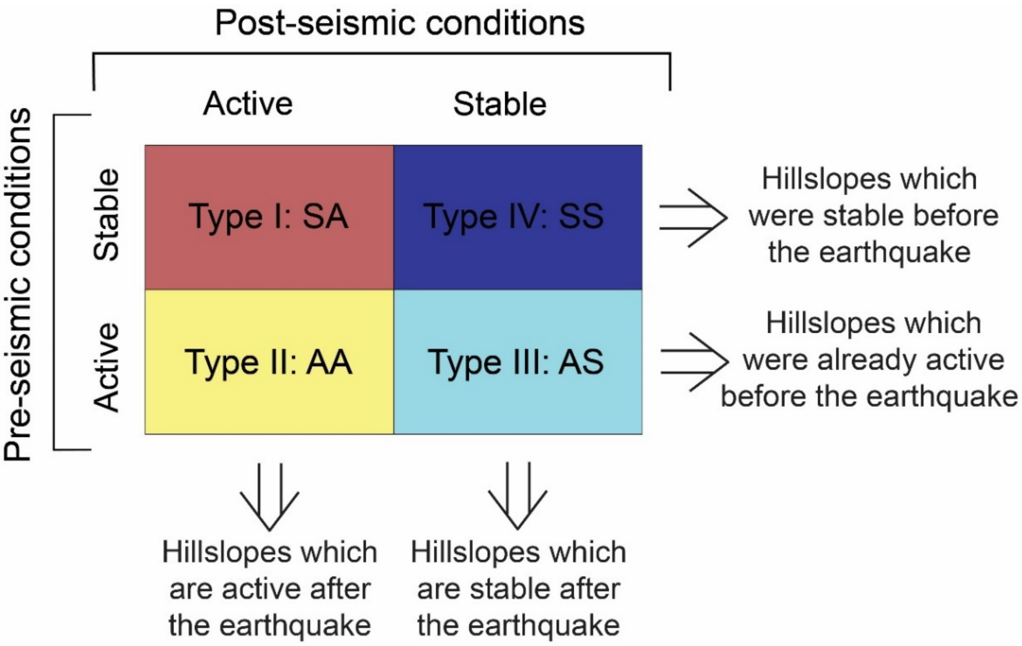

Fig. 3. Activity matrix of hillslopes during pre- and post-Kaikōura phase.

4. Results

4.1. Mean annual LOS velocities (V_{LOS})

By processing 26 interferograms of Sentinel-1 acquisitions for the pre-seismic period, we generated 252,231 PS points where V_{LOS} range from -20.27 mm/yr to 20.08 mm/yr (Fig. 4a). The mean and standard deviation of the average V_{LOS} appear as 0.98 mm/yr and 3.86 mm/yr, respectively (Fig. 4a).

As for the post-seismic period, we generated 134,810 PS points in which V_{LOS} values vary between -54.10 mm/yr and 39.10 mm/yr (Fig. 4b). The mean V_{LOS} is around -1.41 mm/yr, and the standard deviation is about 8.44 mm/yr (Fig. 4b). We used the group of nearly stable PS which exist in both periods to align all PS observations in a common reference grid.

In both cases, the positive values signify those regions of the study area moving toward the sensor (i.e., roughly westward motions), while those parts moving away from the sensor (i.e., roughly eastward motions) have a negative value. Spatial distribution of PS points does not indicate a dramatic difference in V_{LOS} over the study area in the pre-seismic phase, whereas distinctive high deformations (i.e., >20mm/yr) are captured in the post-seismic period, specifically across the mountainous landscape around the rupture zone (e.g., the Seaward Kaikōura Ranges). In the post-seismic phase, relatively high deformations are also pronounced even far from the rupture zone whenever the landscape gets steeper (e.g., across the Inland Kaikōura Range and the northwestern part of the study area). By comparing the PS total amount between pre- and post-phases, Fig. 5 shows an approximately 130% absolute increase in V_{LOS} after the earthquake.

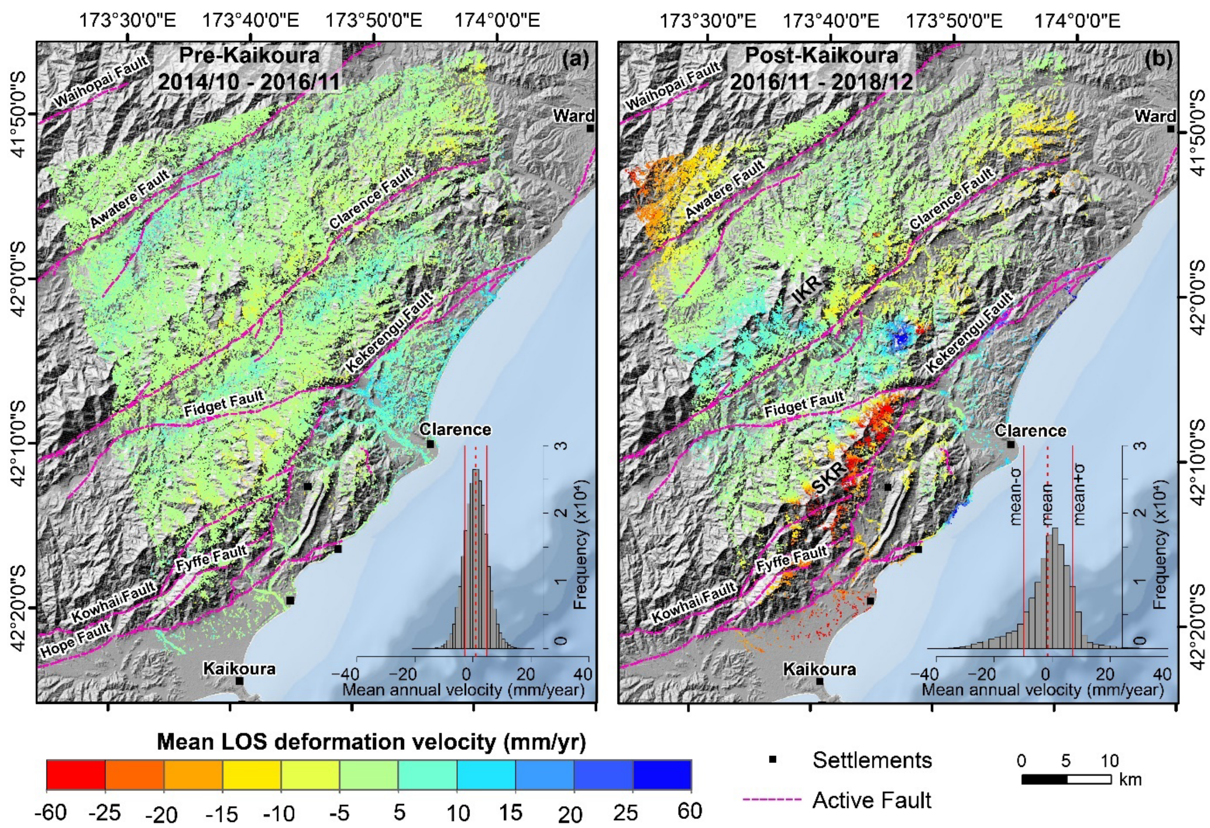

Fig. 4. V_{LOS} before (a) and after (b) the Kaikōura earthquake expressed in mm/yr presented with hillshade generated from DEM. SKR: the Seaward Kaikōura Ranges; IKR: the Inland Kaikōura Range.

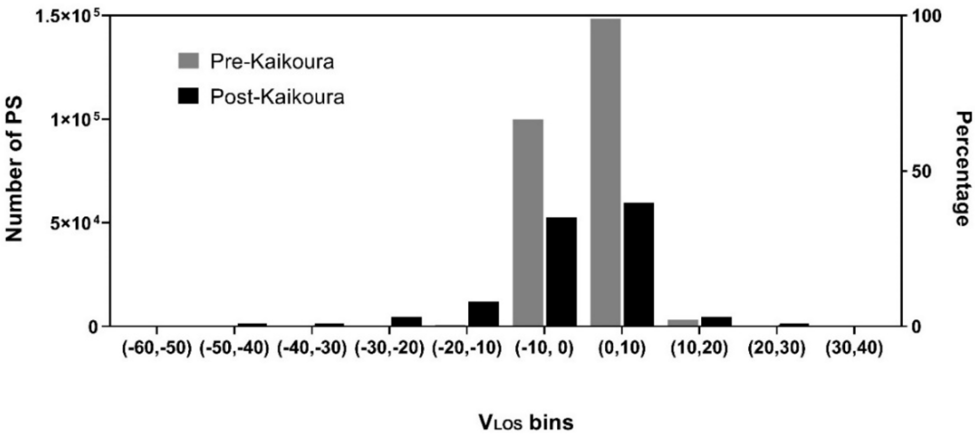

Fig. 5. Comparison of PS point counts during pre- and post-Kaikōura by generating mean annual LOS velocity bins.

Based on the approach described in Methodology section, we labeled actively deforming PS points by setting a critical stability threshold of ±10 mm/yr to V_{LOS}. In the pre-seismic phase, approximately 1% of the PS points are labeled as active. This value increased to ~14% in the post-seismic period. After labeling the active PS, we further classified them into two types namely extremely slow-moving and very slow-moving PS. In the pre-Kaikōura phase, ~99% (2,566) of active PS comes under extremely slow-moving while the rest (33 PS points) is very slow-moving PS. During the post-Kaikōura phase, ~55% (10,641 PS points) and ~45% (8,805 PS points) of PS points are classified as extremely slow-moving and very slow-moving PS, respectively (Fig. 6).

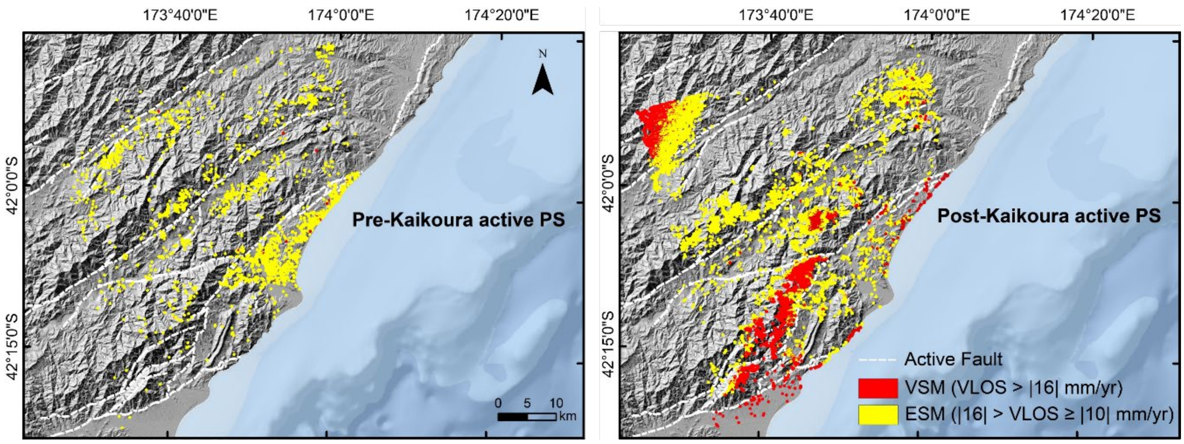

Fig. 6. Spatial distribution of extremely slow-moving (ESM) and very slow-moving (VSM) PS points during pre- and post-Kaikōura periods.

4.2. Morphometric and seismic factors influencing post-seismic V_{LOS}

To understand the variability of PS pixels having different deformation rates, we created ten bins of V_{LOS}, each having a 10 mm/yr interval and examined their variation over different slope steepness and PGA values (Figs. 7a and 7b). Results show a descending pattern in slope steepness from negative to positive surface deformations (Fig. 7a). Median V_{LOS} values are always between 30 and 40 degrees for the PS points experiencing deformations <-20 mm/yr. This observation matches with median slope steepness of coseismic landslides triggered by the Kaikōura earthquake (Tanyas et al., 2022). At the other edge of the spectrum, PS points with V_{LOS}>20 mm/yr appear on gentle hillslopes where median slope steepness is approximately below 20 degrees. In some specific V_{LOS} bins (i.e., 20 mm/yr<V_{LOS}<30 mm/yr) median slope steepness is even less than 10 degrees. Notably, both positive and negative deformation signals might be associated with hillslope motions.

As for the connection between ground shaking and post-seismic deformation, results show that PS having higher deformation either moving away from the satellite (from -40 to -60 mm/yr) or towards the satellite (from 20 to 40 mm/yr) are primarily found in regions that experienced PGA larger than 0.6 g during the earthquake (Fig. 7b). Overall, larger the ground shaking, higher the post-seismic deformation.

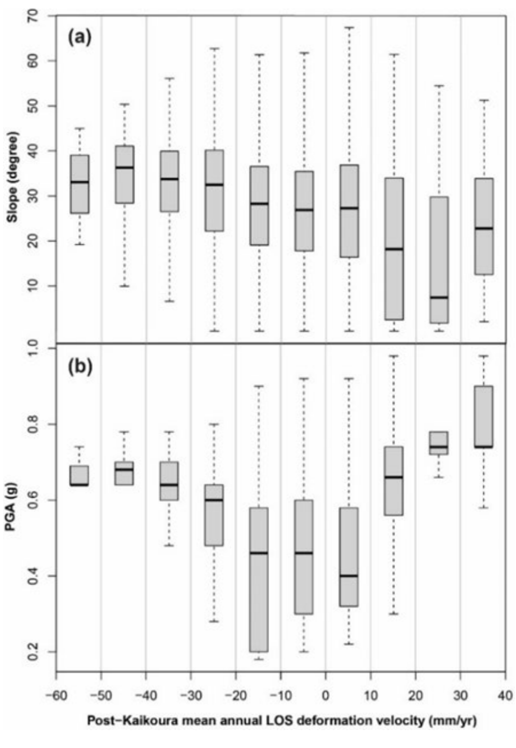

Fig. 7. Box plots showing the variation of the (a) slope steepness, and (b) PGA in response to various bins of V_{LOS} retrieved following the Kaikōura earthquake.

We also examined aspect distribution of PS points (Fig. 8). We focused, in particular, on active PS points. Results show that PS points with deformation signal away from the sensor (i.e., roughly eastward motions) are mainly located on east-northeast facing hillslopes (Fig. 8b), whereas the same link is not pronounced for the PS points where the deformation signal is towards the sensor (Fig. 8c). In fact, in the former case, the aspect of hillslopes with high deformations does not fully match with the dominant aspect of the examined landscape. But it is well in alignment with aspect distribution of coseismic landslides likely associated with the directivity effect of the Kaikōura earthquake (Tanyas et al., 2022). This implies that hillslopes hosting more coseismic landslides due to the earthquake directivity effect also show high post-seismic deformations.

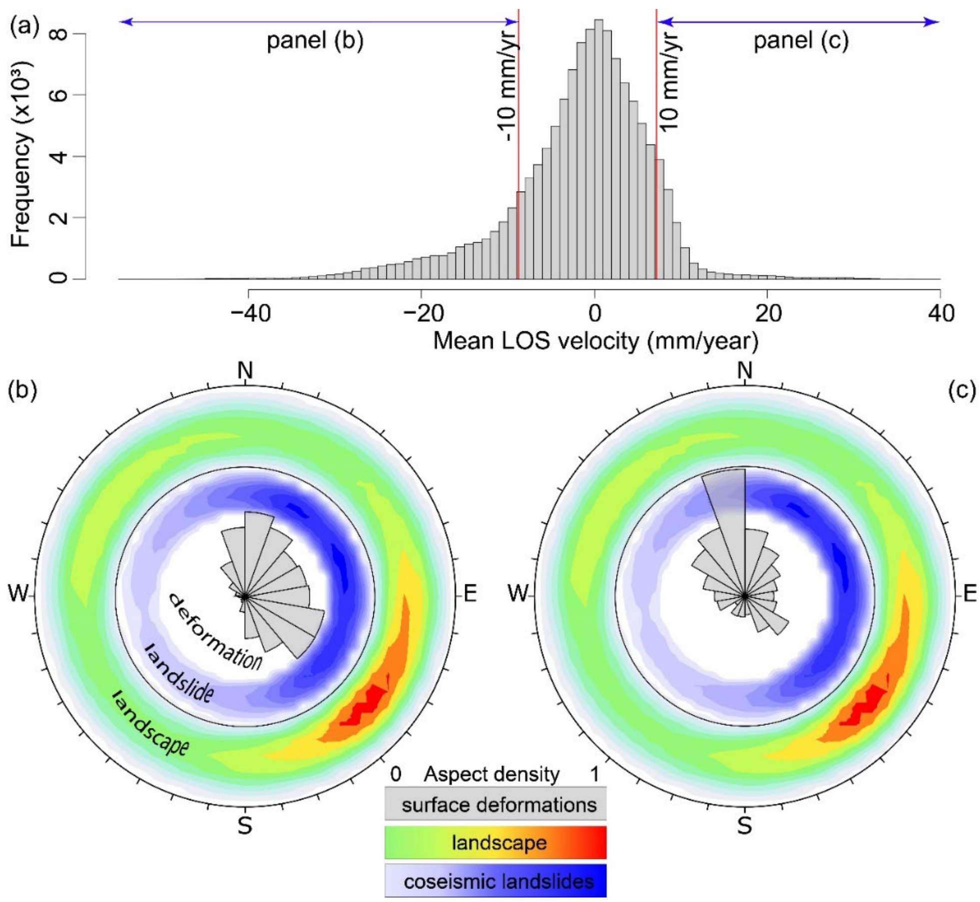

Fig. 8. Rose diagram displaying the pattern of aspect in relation to post-Kaikōura active surface deformations and landslides triggered during the main shock of the Kaikōura earthquake.

4.3. Actively deforming hillslopes and their post-seismic evolutions

To systematically examine actively deforming hillslopes, we aggregated PS points at the level of SUs (see Supplementary Materials, Fig. S6). Actively deforming hillslopes were further classified into extremely slow-moving and very slow-moving hillslopes based on the average

LOS velocity of the hillslopes. By doing so, we labeled nine extremely slow-moving hillslopes in the pre-seismic period between October 2014 and November 2016 (Fig. 9a). After the Kaikōura earthquake, between November 2016 and December 2018, 243 hillslopes were actively deforming (Fig. 9b). Amon those hillslopes, 141 are found to be extremely slow-moving, and 102 are observed as very slow-moving.

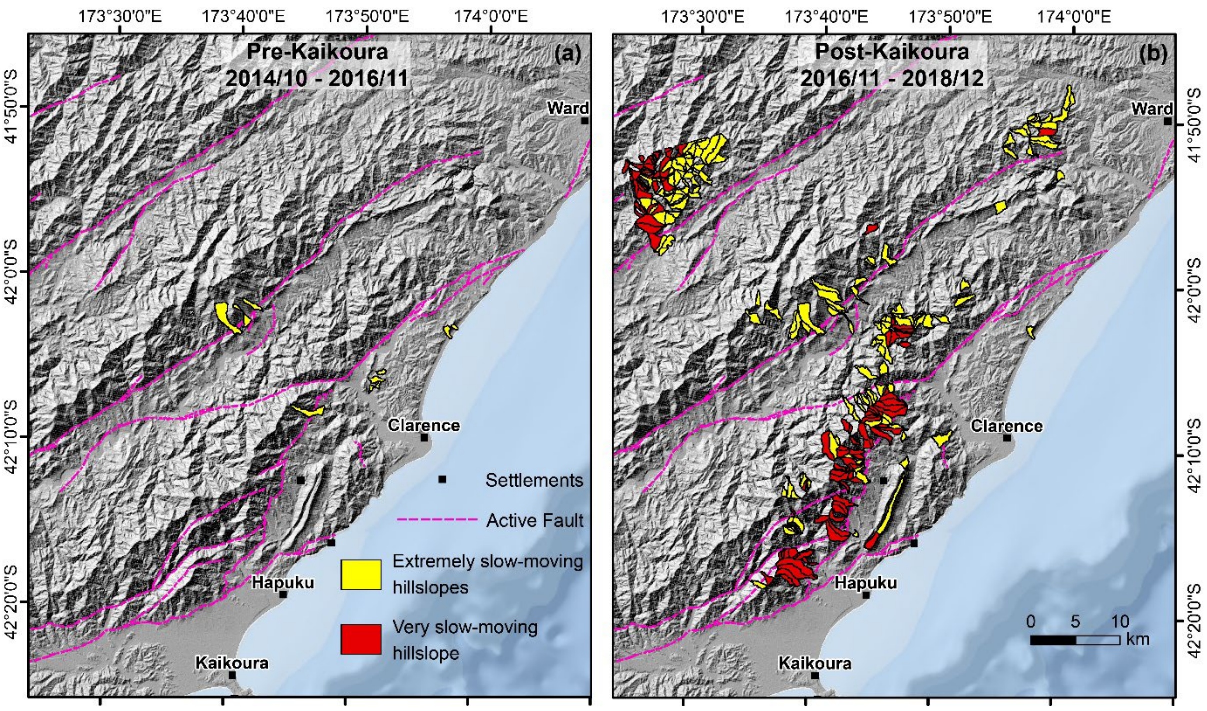

Fig. 9. Actively deforming hillslopes identified during the pre-Kaikōura phase (a) and post-Kaikōura phase (b) superimposed on hillshade generated from DEM.

After labeling active and stable hillslopes, we further examined their evolutions (Fig. 10) based on HDS (see Fig. 3). We did so by calculating the average deformation values of all PS points located in a SU. Below, we examined Type I, II, and III in detail with the deformation time series using one representative hillslope. We did not exemplify Type IV, which refers to stable hillslopes in both pre- and post-seismic phases.

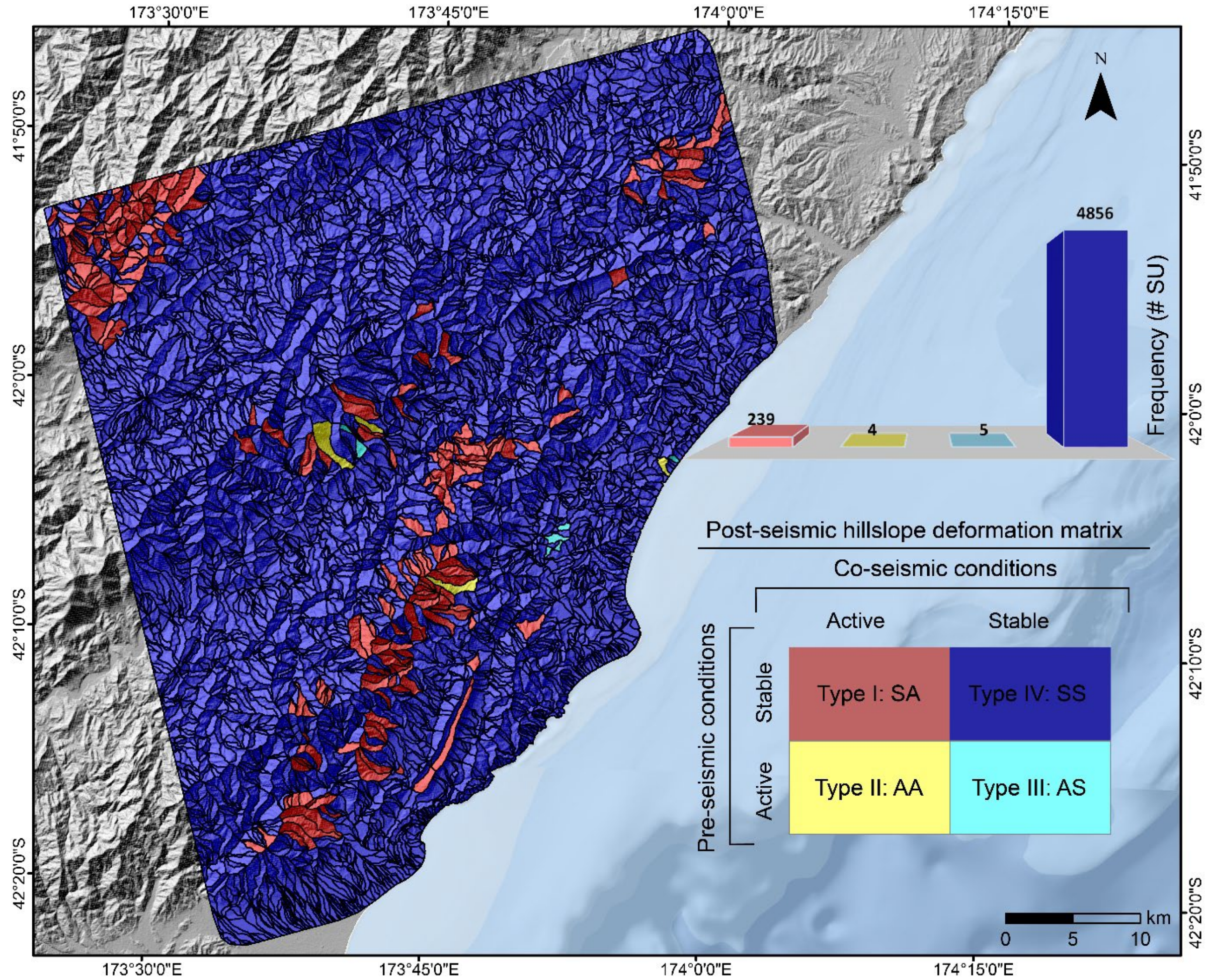

Fig. 10. Four types of sub-meter hillslope deformation activity classes observed in the study area.

4.4.1. Type-I (SA)

Apart from triggering a large number of coseismic landslides, the 2016 Kaikōura earthquake is found to have initiated active deformation in 239 hillslopes across the study area, which were seen to be inactive before the large seismic event. Out of 239 hillslopes, 129 belong to the extremely slow-moving hillslope category, while the rest are very slow-moving hillslopes.

The representative hillslope is located 89 km northeast of the epicenter of the Kaikōura earthquake and just above the Jordan thrust fault, which experienced a significant slip during the 2016 event (Diederichs et al., 2019). The slope gradient of the hillslope ranges between 3° and 60°, and the hillslope has an area of 1.4 km^2. There is a lack of PS coverage over the densely vegetated body and toe of the hillslope owing to the temporal decorrelation. Yet, a small region devoid of vegetation in the body of the hillslope is observed to contain a few PS. Overall, the mean LOS velocity of the hillslope is 2.5 mm/yr during the pre-seismic phase and -31.51 mm/yr after the earthquake (Figure 11).

To understand how the deformation of the hillslope varies in different time steps before and after the 2016 Kaikōura earthquake, the average deformation time series of the entire hillslope as well as one selected PS point (PS_1), one on the scarp region of the hillslope is plotted (Fig. 11). The PS_1 has a mean V_{LOS} of 3.35 mm/yr and -33.99 mm/yr during pre- and post-seismic phases. It can be noted from the linear trend of deformation that the hillslope was inactive during the pre-Kaikōura phase and began to show a sudden increase in the deformation rate after the earthquake (Fig. 11). Also, a gradual decay in the deformation velocity during the post-Kaikōura period is observed from the average deformation time series of the hillslope.

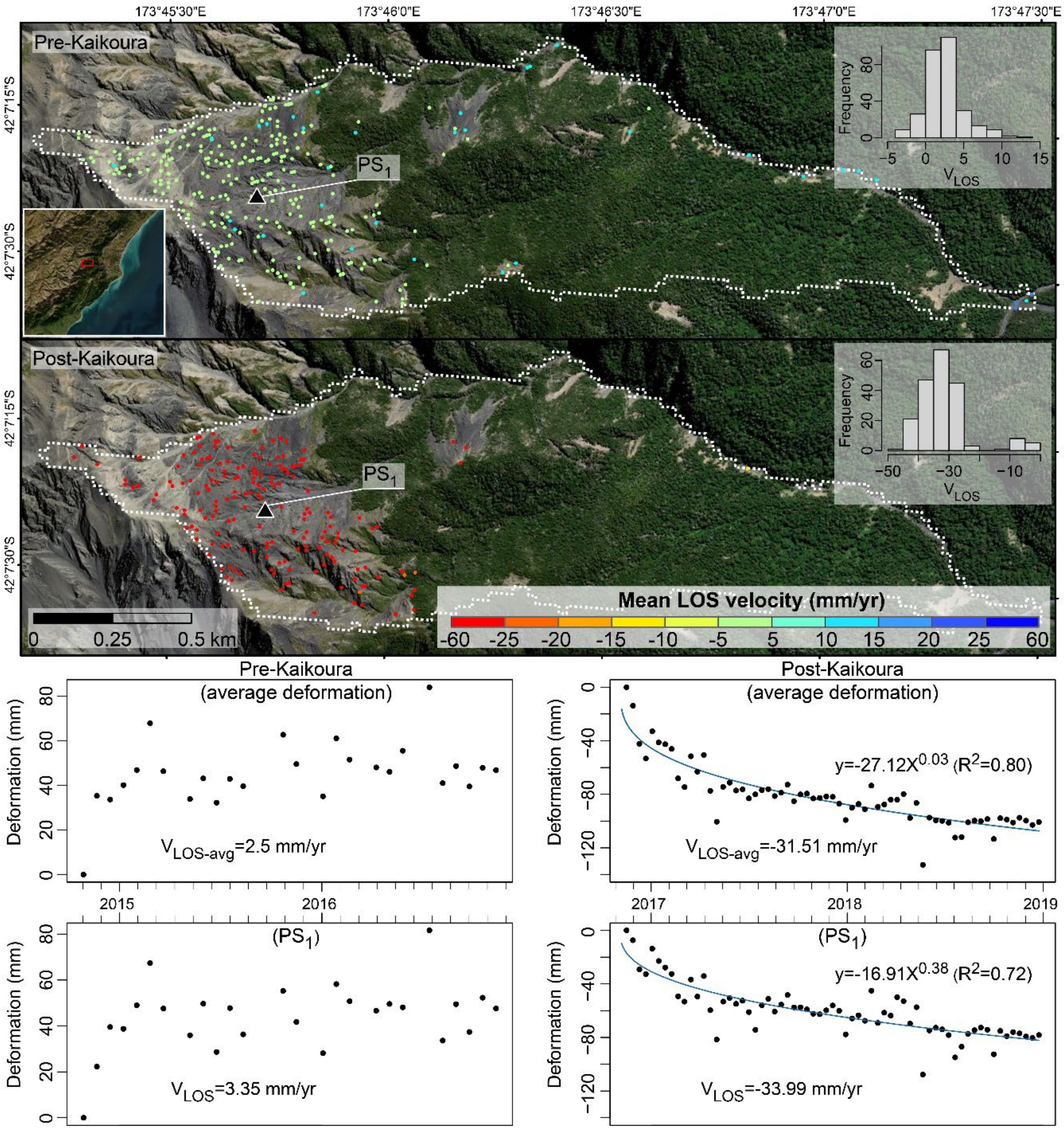

Fig. 11. Hillslope representing Type I: (SA) category of HDS along with deformation time series before and after the Kaikōura earthquake for the entire hillslope and a selected PS point.

4.4.2. Type-II (AA)

We identified four hillslopes with active deformation in pre- and post-seismic phases. The representative hillslope is located 94.5 km away from the earthquake epicenter and has an area of 1.01 km². This hillslope is found to be extremely slow-moving before the earthquake, which continues to be the same after the event but with a change in the deformation velocity. The mean V_{LOS} of the entire hillslope slightly increased from -11.64 mm/yr to -12.12 mm/yr from pre- to post-seismic phases (Fig. 12). In addition, the mean V_{LOS} of a selected PS point (PS_2) is -10.76 mm/yr before the mainshock while the same during the post-seismic phase is -10.61 mm/yr.

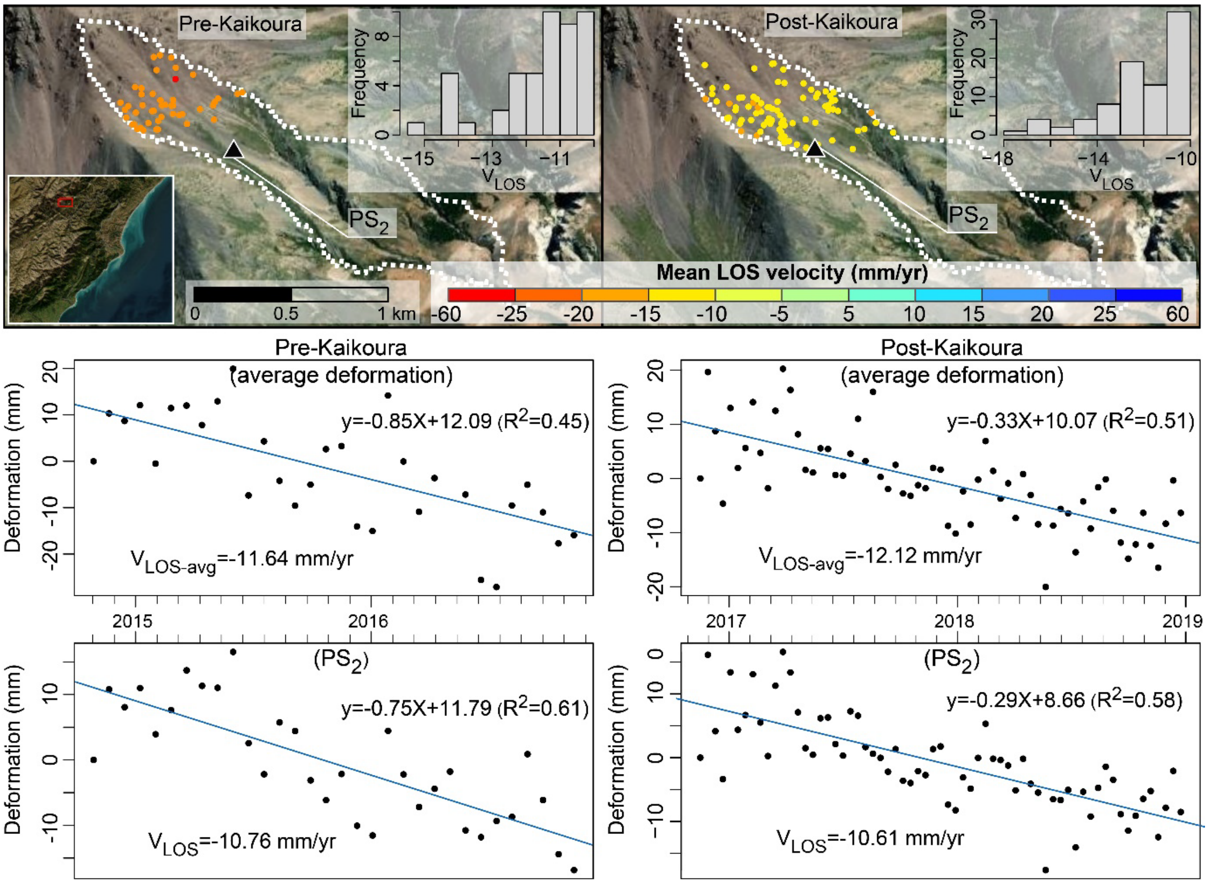

Fig. 12. Hillslope representing Type II: (AA) category of HDS along with deformation time series before and after the Kaikōura earthquake for the entire hillslope and a selected PS pixel.

4.4.3. Type-III (AS)

Five hillslopes are stabilized after the earthquake. The representative hillslope is 98 km northeast of the earthquake's epicenter and has an area of 0.81 km². The hillslope has a positive mean V_{LOS} before and after the earthquake (Fig. 13). However, the hillslope is observed to have extremely slow movement before the earthquake with a mean V_{LOS} of 11.66 mm/yr. In the post-seismic phase, there is a decrease in V_{LOS} to 6.43 mm/yr, which is below the active deformation threshold (see Fig. 13). The same can be observed for the selected PS (PS_3) point before (15.37 mm/yr) and after (5.07 mm/yr) the mainshock.

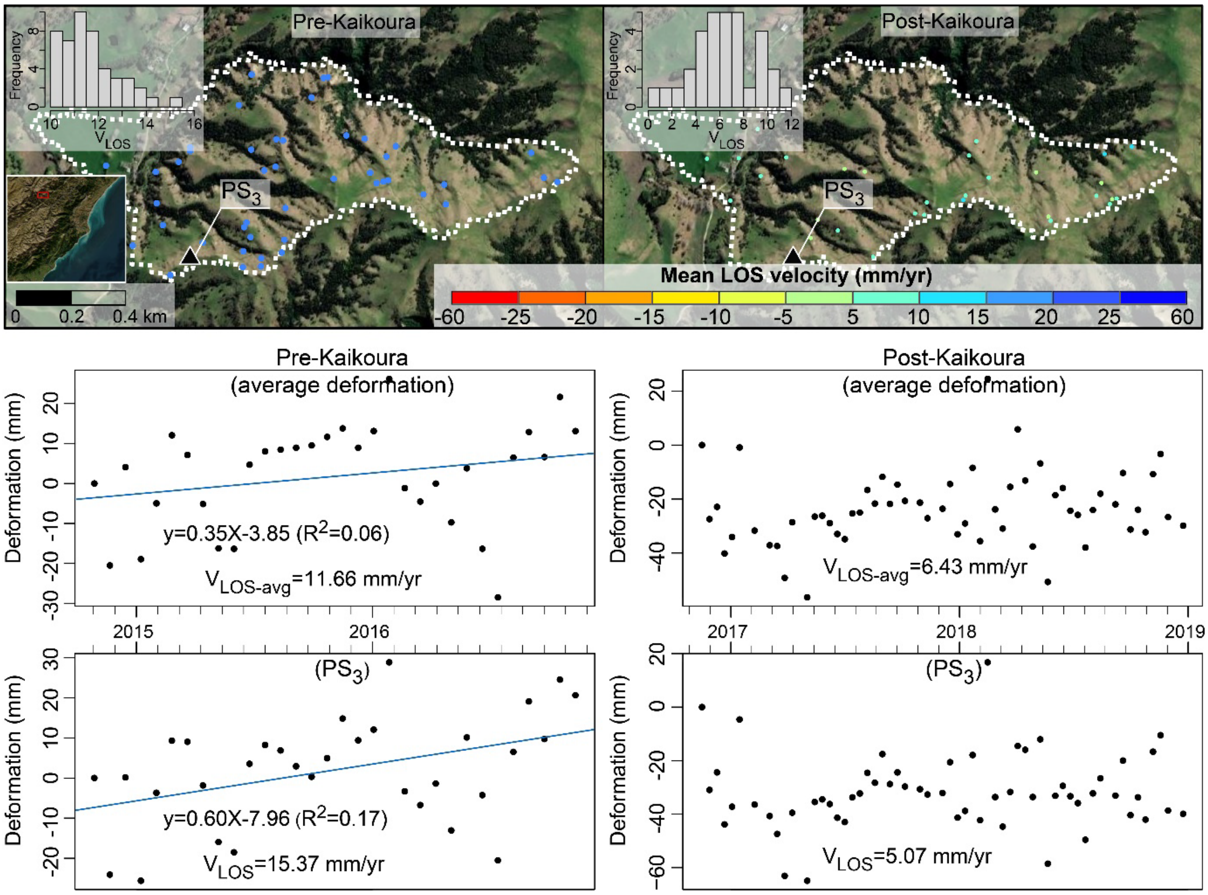

Fig. 13. Representative hillslope for the Type III: (AS) based on the HDS presented along with the deformation time series before and after the mainshock.

4.4.4. Interactions with coseismic landslides

We also checked the spatial distribution of hillslopes associated with both presence of coseismic landslides and active hillslope deformations (Fig. 14). Results show that 127 hillslopes that are found to be actively deforming in the post-Kaikōura phase are already affected by the coseismic landslides. However, 116 actively deforming hillslopes have not failed yet. This implies that in the future, new landslides in these actively deforming hillslopes could be expected.

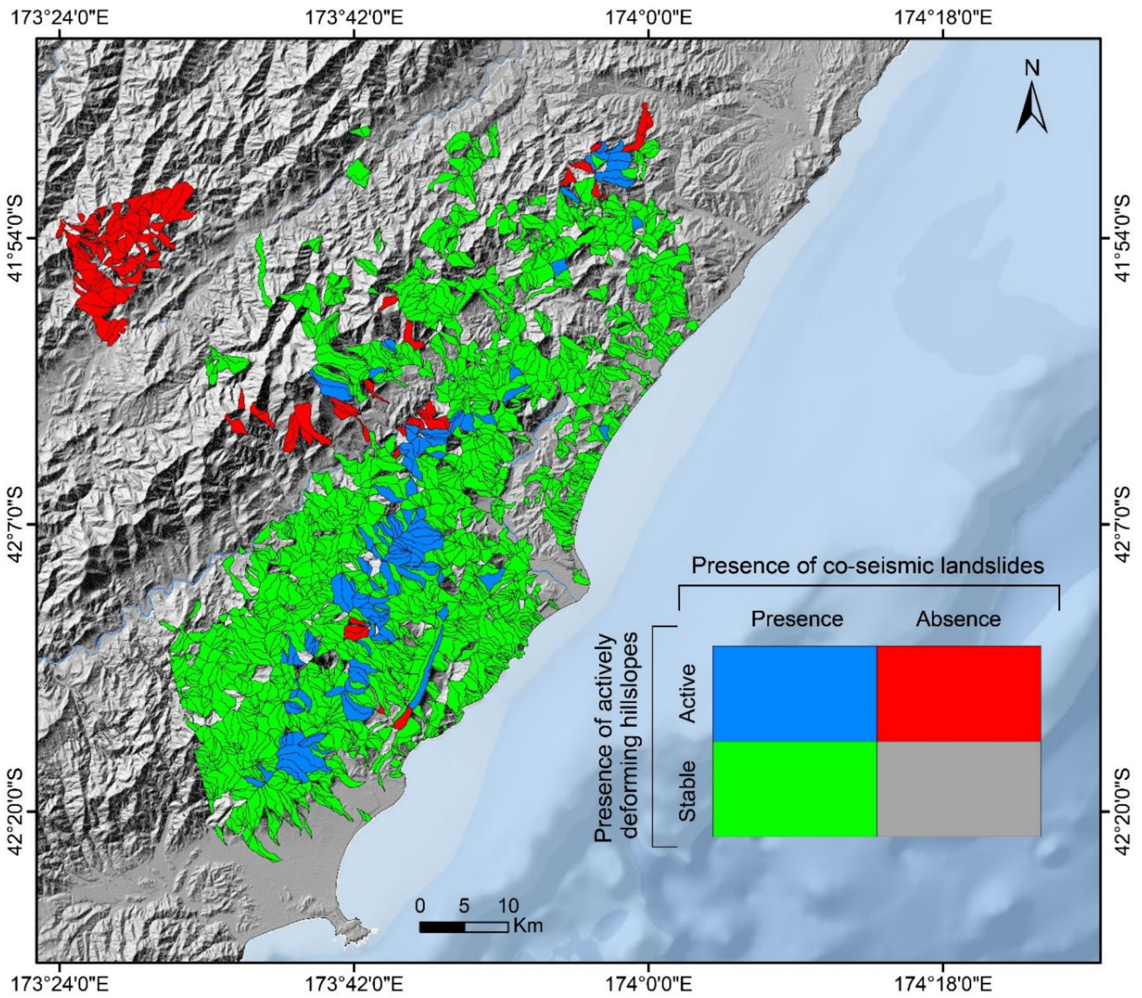

Fig. 14. Different types of actively deforming hillslopes associated with the presence of coseismic landslides.

5. Discussion

Findings of this research offer a comprehensive illustration of how a large-magnitude earthquake alters the deformation patterns of hillslopes.

This was achieved by means of two intrinsically related novelties introduced in this work. First, for the first time, we used SUs to aggregate PS points to identify active hillslopes rather than using the standard pixel density clustering approach (e.g., Bekaert et al., 2020; Aslan et al., 2020). This approach helped us to systematically examined the entire study area and also to develop the post-seismic hillslope evolution matrix, which could be considered as the second novelty of this contribution. The literature shows examples of newly formed slow-moving landslides and/or failure of actively deformed hillslopes associated with strong earthquakes (e.g., Cai et al., 2022; Cheaib et al., 2022; Bekaert et al., 2020). However, we were able to expand such analyses indicating changes in hillslope deformations over the entirety of the examined area as we exploited SUs.

As a result, we developed and showcased a systematic approach for identifying active hillslopes which are already existed before and those that were generated after the impact of the 2016 Kaikōura earthquake. Our results documented an abrupt increase in the number of active deforming hillslopes following the ground shaking. Monitoring of such active hillslopes for a long time can help in making well-informed management decisions to prevent those active slopes from failing catastrophically owing to acceleration from further external triggers (Lacroix et al., 2020).

Among four different hillslope evolution categories described in this research, Type I points out hillslopes began deforming right after an earthquake. This could be interpreted as the genesis of a slow-moving landslide. Such evolution is mainly attributed to the intense seismic shaking, which reduces the strength of the hillslope (Brain et al., 2017). However, in our case, we do not know if those hillslopes were historically active before 2014. Therefore, Type I could also stand for reactivation of previously stabilized slow-moving hillslopes.

5.1. Similarities between abrupt coseismic and slow-moving post-seismic deformations

Our analyses on the spatial distribution of surface deformations over the study area with respect to morphometric and seismic variables provided some new insight helping us to better understand factors governing hillslope deformation in post-seismic periods. In fact, some of those observations showed similarities with variables controlling the spatial distribution of coseismic landslides. For instance, most of the very slow-moving PS detected in the post-Kaikōura phase are concentrated around rupturing zone where the landscape was exposed to higher ground shaking during the 2016 mainshock. Such an observation is also valid for coseismic landslides in general (Petricca et al., 2021; Huang et al., 2017) and specifically for the ones triggered by the 2016 Kaikōura earthquake, as the majority of the landslides occurred close to the fault rupture zone (Massey et al., 2020). In this context, our results show that the earthquake legacy effect is also more persistent on hillslopes exposed to strong ground shaking.

5.2. Limitations

Even though PSI-based sub-meter evolution monitoring and mapping of hillslopes has a good effectiveness, but it also has certain limitations. The first and foremost challenge in using PSI approach is the loss of temporal correlation, which can arise from many factors, including high precipitation, snowfall and growth of vegetation (Bekaert et al., 2020; Hanssen, 2001). This reason inhibited in acquiring PS points over highly vegetated region of the hillslopes while only those scarp regions devoid of vegetation cover and dense snowfall were observed to contain PS (see Figure 49). Such a disadvantage of temporal decorrelation can be reduced by utilising a longer wavelength such as L-band images, which can penetrate through the dense vegetation cover (Xu et al., 2021). However, it should be also noted that shorter wavelength data such as C-band images is extremely responsive in capturing deformation signals (van Natijne et al., 2022). In addition, employing other TS-InSAR techniques such as SBAS can help in increasing the density of captured deformation measurements over space as its characteristics allows selecting temporarily coherent distributed scatterers and point scatterers along with PS (X. Chen et al., 2021).

The second constraint of this research is the unavailability of descending flight direction images of Sentinel-1, which inhibited the decomposition of LOS deformation into horizontal and vertical components. Therefore, this research utilised LOS deformation further to detect active PS in accordance with the hillslope velocity classification of Cruden and Varnes (1996). Such approach is not uncommon as previous studies have also utilised the LOS velocity for identifying active hillslopes (Bayer et al., 2018; Bekaert et al., 2020; Cheaib et al., 2022; Lacroix et al., 2022).

The next challenge is that InSAR is highly effective to detect the deformation that occurs in the LOS direction (Xu et al., 2021). In this study, a large number of hillslopes faces south-east direction while there is also considerable amount of hillslopes that are seen facing north and south direction. In addition, even though InSAR based deformation measurements reported to be in line with those recorded in GNSS stations (Cigna et al., 2021), the unavailability of GNSS station data from the study site to evaluate the reliability of the extracted surface deformation measurement is also a major limitation in this study.

It should also be noted that hillslopes with sub-meter deformations are only identified and monitored in this study. Therefore, those hillslopes that are reported to be stable in this research could also experience rapid movements or failures in the post-seismic phase. This is because sudden meter-level displacement is almost impossible to be accurately detected by PSI. In addition, there are no studies available to our knowledge documenting the post-seismic rapid landsliding in the study area, thus, it is difficult to say if the stable slopes reported in this study are actually stable. In addition, in the post-seismic phase there are active movements that are a mix of tectonic and landsliding related movements, which are not explored.

We did not examine the relationship between the deformation measurements with rainfall, soil moisture, land surface temperature or areal fraction of snow cover as well as various morphometric and/or geologic variables. Possible contribution of these environmental variables should be studied further. Also, this research could be expanded further by investigating scattering types of PS, including surface, volume and double bounce scattering, using multi-polarization SAR data (e.g. Sentinel-1 SAR with VV and VH), which may contribute to better data interpretation. Moreover, artificial intelligence such as recurrent neural network (Kulshrestha et al., 2022) can be used to differentiate actively moving PS from stable ones.

6. Conclusion

This research developed a systematic approach for identifying extremely slow- and very slow-moving hillslopes in post-seismic periods. We integrated the use of slope units in the post-processing of surface deformation measurements and examined the evolution of post-seismic hillslope deformations over the entirety of the study area. We proposed and demonstrated a post-seismic hillslope deformation scheme, which could be applied in other areas affected by earthquakes. In this context, we suggested four hillslope categories: (i) inactive hillslope becoming active (Type I: SA), (ii) active hillslope remaining unaffected with changes in dynamics (Type II: AA), (iii) active hillslope that have become inactive (Type III: AS) and (iv) those hillslopes that are stable prior and following the earthquake (Type IV: SS)

Specifically, we examined pre- and post- seismic hillslope deformations in the area affected by the 2016 Kaikōura earthquake and monitored their sub-meter evolution using freely available Sentinel-1 images through the PSI approach. The extracted surface deformations showed an abrupt increase in deformations following the intense ground shaking and then a gradual decrease in the following post-seismic periods from November 2016 to December 2018. Overall, the sharp increase in the number of stable hillslopes that started moving extremely slowly and very slowly after the impact of the 2016 Kaikōura earthquake and their deformation dynamics there after confirms the firm role of earthquake legacy effect on their evolution. Spatial distribution of hillslope deformations also showed that the regions affected by higher ground shaking exhibited also higher deformation in the post-seismic phase compared to hillslopes affected by lower seismic shaking.

Acknowledgments

We express our thanks to Prof. Dr. Cees Van Westen for his advice and helpful comments. The Geospatial Computing Platform of the Center of Expertise in Big Geodata Science (CRIB) (https://crib.utwente.nl) is used for the processing of Sentinel-1 data. We thank Dr. Serkan Girgin for his support in providing the necessary computing infrastructure. In addition, we also thank Dr. Islam Fadel for his support with Sentinel-1 data processing.

Data availability

All data used in this research was collected from publicly available data sources.

Author contribution

NS, HT and LC: Conceptualisation, Research design. **NS, HT:** Methodology, Software, Visualisation. **NS:** Data curation, Formal analysis, Investigation. **LC and HT**: Supervision. **NS:** Writing- Original draft preparation. **HT and LC:** Writing- Reviewing and Editing.

Competing interests

The authors declare no competing interest.

References

Alvioli, M., Mondini, A.C., Fiorucci, F., Cardinali, M., Marchesini, I., 2018. Topography-driven satellite imagery analysis for landslide mapping. Geomatics, Natural Hazards and Risk 9, 544–567. https://doi.org/10.1080/19475705.2018.1458050

Aslan, G., Foumelis, M., Raucoules, D., de Michele, M., Bernardie, S., Cakir, Z., 2020. Landslide mapping and monitoring using persistent scatterer interferometry (PSI) technique in the French alps. Remote Sens (Basel) 12. https://doi.org/10.3390/RS12081305

Bamler, R., Hartl, P., 1998. Synthetic aperture radar interferometry. Inverse Probl 14, R1. https://doi.org/10.1088/0266-5611/14/4/001

Bayer, B., Simoni, A., Mulas, M., Corsini, A., Schmidt, D., 2018. Deformation responses of slow moving landslides to seasonal rainfall in the Northern Apennines, measured by InSAR. Geomorphology 308, 293–306. https://doi.org/10.1016/j.geomorph.2018.02.020

Bayer, B., Simoni, A., Schmidt, D., Bertello, L., 2017. Using advanced InSAR techniques to monitor landslide deformations induced by tunneling in the Northern Apennines, Italy. Eng Geol 226, 20–32. https://doi.org/10.1016/j.enggeo.2017.03.026

Bekaert, D.P.S., Handwerger, A.L., Agram, P., Kirschbaum, D.B., 2020. InSAR-based detection method for mapping and monitoring slow-moving landslides in remote regions with steep and mountainous terrain: An application to Nepal. Remote Sens Environ 249, 111983. https://doi.org/10.1016/j.rse.2020.111983

Bekaert, D.P.S., Hooper, A., Wright, T.J., 2015. A spatially variable power law tropospheric correction technique for InSAR data. J Geophys Res Solid Earth 120, 1345–1356. https://doi.org/10.1002/2014JB011558

Berardino, P., Fornaro, G., Lanari, R., Sansosti, E., 2002. A new algorithm for surface deformation monitoring based on small baseline differential SAR interferograms. IEEE Transactions on Geoscience and Remote Sensing 40, 2375–2383. https://doi.org/10.1109/TGRS.2002.803792

Blasco, J.M.D., Fernandez, D., Foumelis, M., Blasco, J.D., Desnos, Y.-L., Engdahl, M., Fernández, D., Veci, L., Lu, J., Wong, C., 2018. ESA SNAP – Stamps integrated processing for sentinel-1 persistent scatterer interferometry, in: International Geoscience and Remote Sensing Symposium (IGARSS). IEEE, pp. 1364–1367. https://doi.org/10.1109/IGARSS.2018.8519545

Bradley, B., Comerio, M., Cubrinovski, M., Dellow, S., Dizhur, D., Elwood, K., Giaretton, M., Green, R., Horspool, N., Hughes, M., Ingham, J., Johnson, L., Massey, C., Seville, E., Simkin, G., Stevenson, J., Wilson, R., Wotherspoon, L., 2017. M7. 8 Kaikoura, New Zealand Earthquake on November 14, 2016.

Brain, M.J., Rosser, N.J., Tunstall, N., 2017. The control of earthquake sequences on hillslope stability. Geophys Res Lett 44, 865–872. https://doi.org/10.1002/2016GL071879

Cai, J., Zhang, L., Dong, J., Dong, X., Li, M., Xu, Q., Liao, M., 2022. Detection and characterization of slow-moving landslides in the 2017 Jiuzhaigou earthquake area by combining satellite SAR observations and airborne Lidar DSM. Eng Geol 305, 106730. https://doi.org/10.1016/J.ENGGEO.2022.106730

Cao, Y., Hamling, I., Massey, C., Upton, P., 2022. Slow-moving landslides triggered by the 2016 Mw 7.8 Kaikōura earthquake, New Zealand: a new InSAR phase-gradient based time-series approach. https://doi.org/10.1002/ESSOAR.10512014.1

Cheaib, A., Lacroix, P., Zerathe, S., Jongmans, D., Ajorlou, N., Doin, M.P., Hollingsworth, J., Abdallah, C., 2022. Landslides induced by the 2017 Mw7.3 Sarpol Zahab earthquake (Iran). Landslides 19, 603–619. https://doi.org/10.1007/S10346-021-01832-0/FIGURES/10

Chen, M., Tang, C., Wang, X., Xiong, J., Shi, Q., Zhang, X., Li, M., Luo, Y., Tie, Y., Feng, Q., 2021. Temporal and spatial differentiation in the surface recovery of post-seismic landslides in Wenchuan earthquake-affected areas. Ecol Inform 64, 101356. https://doi.org/10.1016/J.ECOINF.2021.101356

Chen, X., Tessari, G., Fabris, M., Achilli, V., Floris, M., 2021. Comparison Between PS and SBAS InSAR Techniques in Monitoring Shallow Landslides 155–161. https://doi.org/10.1007/978-3-030-60311-3_17

Cigna, F., Bianchini, S., Casagli, N., 2013. How to assess landslide activity and intensity with Persistent Scatterer Interferometry (PSI): The PSI-based matrix approach. Landslides 10, 267–283. https://doi.org/10.1007/S10346-012-0335-7/FIGURES/11

Cigna, F., Ramírez, R.E., Tapete, D., 2021. Accuracy of Sentinel-1 PSI and SBAS InSAR Displacement Velocities against GNSS and Geodetic Leveling Monitoring Data. Remote Sensing 2021, Vol. 13, Page 4800 13, 4800. https://doi.org/10.3390/RS13234800

Colesanti, C., Ferretti, A., Prati, C., Rocca, F., 2003. Monitoring landslides and tectonic motions with the Permanent Scatterers Technique. Eng Geol 68, 3–14. https://doi.org/10.1016/S0013-7952(02)00195-3

Colesanti, C., Wasowski, J., 2006. Investigating landslides with space-borne Synthetic Aperture Radar (SAR) interferometry. Eng Geol 88, 173–199. https://doi.org/10.1016/j.enggeo.2006.09.013

Cruden, D., Varnes, D., 1996. Landslide types and processes, in: Turner, A., Schuster, R. (Eds.), Landslides Investigation and Mitigation. ransportation research board, US National Research Council, Washington, DC, pp. 36–75.

Duputel, Z., Rivera, L., 2017. Long-period analysis of the 2016 Kaikoura earthquake. Physics of the Earth and Planetary Interiors 265, 62–66. https://doi.org/10.1016/J.PEPI.2017.02.004

Fan, X., Scaringi, G., Korup, O., West, A.J., van Westen, C.J., Tanyas, H., Hovius, N., Hales, T.C., Jibson, R.W., Allstadt, K.E., Zhang, L., Evans, S.G., Xu, C., Li, G., Pei, X., Xu, Q., Huang, R., 2019. Earthquake-Induced Chains of Geologic Hazards: Patterns, Mechanisms, and Impacts. Reviews of Geophysics 57, 421–503. https://doi.org/10.1029/2018RG000626

Ferretti, A., Prati, C., Rocca, F., 2001. Permanent scatterers in SAR interferometry. IEEE Transactions on Geoscience and Remote Sensing 39, 8–20. https://doi.org/10.1109/36.898661

Fruneau, B., Achache, J., Delacourt, C., 1996. Observation and modelling of the Saint-Étienne-de-Tinée landslide using SAR interferometry. Tectonophysics 265, 181–190. https://doi.org/10.1016/S0040-1951(96)00047-9

Guzzetti, F., Reichenbach, P., Cardinali, M., Galli, M., Ardizzone, F., 2005. Probabilistic landslide hazard assessment at the basin scale. Geomorphology 72, 272–299. https://doi.org/10.1016/J.GEOMORPH.2005.06.002

Hamling, I.J., Hreinsdóttir, S., Clark, K., Elliott, J., Liang, C., Fielding, E., Litchfield, N., Villamor, P., Wallace, L., Wright, T.J., D'Anastasio, E., Bannister, S., Burbidge, D., Denys, P., Gentle, P., Howarth, J., Mueller, C., Palmer, N., Pearson, C., Power, W., Barnes, P., Barrell, D.J.A., van Dissen, R., Langridge, R., Little, T., Nicol, A., Pettinga, J., Rowland, J., Stirling, M., 2017. Complex multifault rupture during the 2016 Mw 7.8 Kaikōura earthquake, New Zealand. Science (1979) 356. https://doi.org/10.1126/SCIENCE.AAM7194/SUPPL_FILE/HAMLING.SM.PDF

Handwerger, A.L., Roering, J.J., Schmidt, D.A., Rempel, A.W., 2015. Kinematics of earthflows in the Northern California Coast Ranges using satellite interferometry. Geomorphology 246, 321–333. https://doi.org/10.1016/j.geomorph.2015.06.003

Hanssen, R.F., 2001. Radar Interferometry: Data Interpretation and Error Analysis, 1st ed, Remote Sensing and Digital Image Processing. Springer Netherlands, Dordrecht. https://doi.org/10.1007/0-306-47633-9

Hilley, G.E., Bürgmann, R., Ferretti, A., Novali, F., Rocca, F., 2004. Dynamics of slow-moving landslides from permanent scatterer analysis. Science (1979) 304, 1952–1955. https://doi.org/10.1126/science.1098821

Hooper, A., Bekaert, D., Spaans, K., Arikan, M., 2012. Recent advances in SAR interferometry time series analysis for measuring crustal deformation. Tectonophysics 514–517, 1–13. https://doi.org/10.1016/J.TECTO.2011.10.013

Hooper, A., Zebker, H., Segall, P., Kampes, B., 2004. A new method for measuring deformation on volcanoes and other natural terrains using InSAR persistent scatterers. Geophys Res Lett 31, 1–5. https://doi.org/10.1029/2004GL021737

Hooper, A.J., 2008. A multi-temporal InSAR method incorporating both persistent scatterer and small baseline approaches. Geophys Res Lett 35. https://doi.org/10.1029/2008GL034654

Kincey, M.E., Rosser, N.J., Robinson, T.R., Densmore, A.L., Shrestha, R., Pujara, D.S., Oven, K.J., Williams, J.G., Swirad, Z.M., 2021. Evolution of Coseismic and Post-seismic Landsliding After the 2015 Mw 7.8 Gorkha Earthquake, Nepal. J Geophys Res Earth Surf 126, e2020JF005803. https://doi.org/10.1029/2020JF005803

Kulshrestha, A., Chang, L., Stein, A., 2022. Use of LSTM for Sinkhole-Related Anomaly Detection and Classification of InSAR Deformation Time Series. IEEE J Sel Top Appl Earth Obs Remote Sens 15, 4559–4570. https://doi.org/10.1109/JSTARS.2022.3180994

Lacroix, P., Gavillon, T., Bouchant, C., Lavé, J., Mugnier, J.-L., Dhungel, S., Vernier, F., 2022. SAR and optical images correlation illuminates post-seismic landslide motion after the Mw 7.8 Gorkha earthquake (Nepal). Scientific Reports 2022 12:1 12, 1–13. https://doi.org/10.1038/s41598-022-10016-2

Lacroix, P., Handwerger, A.L., Bièvre, G., 2020. Life and death of slow-moving landslides. Nat Rev Earth Environ 1, 404–419. https://doi.org/10.1038/s43017-020-0072-8

López-Vinielles, J., Fernández-Merodo, J.A., Ezquerro, P., García-Davalillo, J.C., Sarro, R., Reyes-Carmona, C., Barra, A., Navarro, J.A., Krishnakumar, V., Alvioli, M., Herrera, G., 2021. Combining Satellite InSAR, Slope Units and Finite Element Modeling for Stability Analysis in Mining Waste Disposal Areas. Remote Sensing 2021, Vol. 13, Page 2008 13, 2008. https://doi.org/10.3390/RS13102008

Marano, K.D., Wald, D.J., Allen, T.I., 2009. Global earthquake casualties due to secondary effects: a quantitative analysis for improving rapid loss analyses. Natural Hazards 2009 52:2 52, 319–328. https://doi.org/10.1007/S11069-009-9372-5

Martino, S., Fiorucci, M., Marmoni, G.M., Casaburi, L., Antonielli, B., Mazzanti, P., 2022. Increase in landslide activity after a low-magnitude earthquake as inferred from DInSAR interferometry. Scientific Reports 2022 12:1 12, 1–19. https://doi.org/10.1038/s41598-022-06508-w

Massey, C.I., Townsend, D.T., Lukovic, B., Morgenstern, R., Jones, K., Rosser, B., de Vilder, S., 2020. Landslides triggered by the MW7.8 14 November 2016 Kaikōura earthquake: an update. Landslides 17, 2401–2408. https://doi.org/10.1007/S10346-020-01439-X/FIGURES/7

McColl, S.T., 2022. Landslide causes and triggers. Landslide Hazards, Risks, and Disasters 13–41. https://doi.org/10.1016/B978-0-12-818464-6.00011-1

Meisina, C., Zucca, F., Fossati, D., Ceriani, M., Allievi, J., 2006. Ground deformation monitoring by using the Permanent Scatterers Technique: The example of the Oltrepo Pavese (Lombardia, Italy). Eng Geol 88, 240–259. https://doi.org/10.1016/J.ENGGEO.2006.09.010

Notti, D., Herrera, G., Bianchini, S., Meisina, C., García-Davalillo, J.C., Zucca, F., 2014. A methodology for improving landslide PSI data analysis. https://doi.org/10.1080/01431161.2014.889864 35, 2186–2214. https://doi.org/10.1080/01431161.2014.889864

Parker, R.N., Hancox, G.T., Petley, D.N., Massey, C.I., Densmore, A.L., Rosser, N.J., 2015. Spatial distributions of earthquake-induced landslides and hillslope preconditioning in the northwest South Island, New Zealand. Earth Surface Dynamics 3, 501–525. https://doi.org/10.5194/ESURF-3-501-2015

Petley, D., Dunning, S., Rosser, N., Kausar, A.B., 2010. Incipient Landslides in the Jhelum Valley, Pakistan Following the 8th October 2005 Earthquake, in: SAARC Workshop on Landslide Risk Management in South Asia. SAARC Disaster Management Centre, Thimpu, Bhutan, pp. 107–116.

Petricca, P., Bignami, C., Doglioni, C., 2021. The epicentral fingerprint of earthquakes marks the coseismically activated crustal volume. Earth Sci Rev 218, 103667. https://doi.org/10.1016/J.EARSCIREV.2021.103667

Raspini, F., Bianchini, S., Ciampalini, A., del Soldato, M., Solari, L., Novali, F., del Conte, S., Rucci, A., Ferretti, A., Casagli, N., 2018. Continuous, semi-automatic monitoring of ground deformation using Sentinel-1 satellites. Scientific Reports 2018 8:1 8, 1–11. https://doi.org/10.1038/s41598-018-25369-w

Rosser, N., Kincey, M., Oven, K., Densmore, A., Robinson, T., Pujara, D.S., Shrestha, R., Smutny, J., Gurung, K., Lama, S., Dhital, M.R., 2021. Changing significance of landslide Hazard and risk after the 2015 Mw 7.8 Gorkha, Nepal Earthquake. Progress in Disaster Science 10, 100159. https://doi.org/10.1016/J.PDISAS.2021.100159

Tang, C., van Westen, C.J., Tanyas, H., Jetten, V.G., 2016. Analysing post-earthquake landslide activity using multi-temporal landslide inventories near the epicentral area of the 2008 Wenchuan earthquake. Natural Hazards and Earth System Sciences 16, 2641–2655. https://doi.org/10.5194/NHESS-16-2641-2016

Tantianuparp, P., Shi, X., Zhang, L., Balz, T., Liao, M., 2013. Characterization of Landslide Deformations in Three Gorges Area Using Multiple InSAR Data Stacks. Remote Sensing 2013, Vol. 5, Pages 2704-2719 5, 2704–2719. https://doi.org/10.3390/RS5062704

Tanyaş, H., Görüm, T., Fadel, I., Yıldırım, C., Lombardo, L., 2022. An open dataset for landslides triggered by the 2016 Mw 7.8 Kaikōura earthquake, New Zealand. Landslides 2022 19:6 19, 1405–1420. https://doi.org/10.1007/S10346-022-01869-9

Tanyaş, H., Kirschbaum, D., Görüm, T., van Westen, C.J., Lombardo, L., 2021a. New Insight into Post-seismic Landslide Evolution Processes in the Tropics. Front Earth Sci (Lausanne) 9, 551. https://doi.org/10.3389/FEART.2021.700546/BIBTEX

Tanyaş, H., Kirschbaum, D., Görüm, T., van Westen, C.J., Tang, C., Lombardo, L., 2021b. A closer look at factors governing landslide recovery time in post-seismic periods. Geomorphology 391, 107912. https://doi.org/10.1016/J.GEOMORPH.2021.107912

Ulrich, T., Gabriel, A.A., Ampuero, J.P., Xu, W., 2019. Dynamic viability of the 2016 Mw 7.8 Kaikōura earthquake cascade on weak crustal faults. Nature Communications 2019 10:1 10, 1–16. https://doi.org/10.1038/s41467-019-09125-w

van Natijne, A.L., Bogaard, T.A., van Leijen, F.J., Hanssen, R.F., Lindenbergh, R.C., 2022. World-wide InSAR sensitivity index for landslide deformation tracking. International Journal of Applied Earth Observation and Geoinformation 111, 102829. https://doi.org/10.1016/J.JAG.2022.102829

Wang, X., Mao, H., 2022. Spatio-temporal evolution of post-seismic landslides and debris flows: 2017 M s 7.0 Jiuzhaigou earthquake. Environmental Science and Pollution Research 29, 15681–15702. https://doi.org/10.1007/S11356-021-16789-9/TABLES/5

Wasowski, J., Bovenga, F., 2014a. Investigating landslides and unstable slopes with satellite Multi Temporal Interferometry: Current issues and future perspectives. Eng Geol. https://doi.org/10.1016/j.enggeo.2014.03.003

Wasowski, J., Bovenga, F., 2014b. Investigating landslides and unstable slopes with satellite Multi Temporal Interferometry: Current issues and future perspectives. Eng Geol. https://doi.org/10.1016/j.enggeo.2014.03.003

Worden, C.B., Wald, D.J., 2016. ShakeMap manual online: Technical manual, user's guide, and software guide. US Geol. Surv. https://doi. org/10.5066/F7D21VPQ.

Xu, Y., Schulz, W.H., Lu, Z., Kim, J., Baxtrom, K., 2021. Geologic controls of slow-moving landslides near the US West Coast. Landslides 18, 3353–3365. https://doi.org/10.1007/S10346-021-01732-3/FIGURES/8

Yang, W., Qi, W., Wang, M., Zhang, J., Zhang, Y., 2017. Spatial and temporal analyses of post-seismic landslide changes near the epicentre of the Wenchuan earthquake. Geomorphology 276, 8–15. https://doi.org/10.1016/J.GEOMORPH.2016.10.010

Yu, C., Li, Z., Penna, N.T., Crippa, P., 2018. Generic Atmospheric Correction Model for Interferometric Synthetic Aperture Radar Observations. J Geophys Res Solid Earth 123, 9202–9222. https://doi.org/10.1029/2017JB015305

Zhao, C., Kang, Y., Zhang, Q., Lu, Z., Li, B., 2018. Landslide Identification and Monitoring along the Jinsha River Catchment (Wudongde Reservoir Area), China, Using the InSAR

Method. Remote Sensing 2018, Vol. 10, Page 993 10, 993. https://doi.org/10.3390/RS10070993